Journal of Physics: Conference Series **2767** (2024) 092100 doi:10.1088/1742-6596/2767/9/092100

Near-wake measurements and simulations of a floating wind turbine using a four-beam nacelle-based lidar

Umut Özinan[1], Moritz Gräfe[1], Christian W. Schulz[2], Po Wen Cheng[1]

[1]Stuttgart Wind Energy, University of Stuttgart, Allmandring 5b, 70569 Stuttgart, Germany
[2]Institute for Fluid Dynamics and Ship Theory, Hamburg University of Technology, Am Schwarzenberg-Campus 4, 21073 Hamburg, Germany

E-mail: oezinan@ifb.uni-stuttgart.de

Abstract. Recent advances in lidar technology have expanded the possibilities for measuring full-scale wind turbine wakes within the atmospheric boundary layer. This study utilizes a four-beam pulsed lidar installed on the nacelle of a floating turbine to measure the near-wake. The wake measurement campaign was conducted on the Floatgen, with lidar measurements reaching up to 2.5 times the rotor diameter distance. These measurements are presented as 10-minute average radial wind speeds. The focus of this study is on the below rated wind speed of 7 m/s. Free flow conditions were assumed at the farthest measurement points, which are located ±0.9 times the rotor diameter from to the rotor center. The sensitivity of lidar measurements to turbulence intensity, vertical wind shear, and significant wave height was investigated. The environmental conditions were categorized into five cases, considering turbulence, vertical shear, and yaw misalignment as well as waves. Two simulation models with different fidelity levels are used to simulate these cases, and the beam-wise radial wind speed predictions are compared with the measurements. A maximum mean absolute error of 11.3% between the measurements and simulations is observed.

1 Introduction

Capturing the wake of a wind turbine in a simulation model is crucial for understanding and optimizing the performance of wind farms, particularly when an accurate estimate of energy production is needed. While the impact of modeling the near-wake on energy production may not be comparable to the far-wake, it plays a vital role in understanding wake development and its evolution into the far-wake. Wind farm simulation tools, such as FAST.Farm[1], utilize the near-wake dynamics to predict the far-wake. Hence, capturing the near-wake becomes crucial, not only for its accurate estimation but also for improving far-wake predictions.

The calibration of wake models is a common step in engineering wake models, where quick estimates of wakes are needed. These models often require the adjustment of empirical parameters based on experimental measurements, large-eddy simulations (LES), or real-world data. In [2], various analytical wake models were tuned and compared to wind tunnel tests, considering wake deficit, deflection, and added turbulence intensity (TI). When dealing with floating offshore wind turbines (FOWTs), additional dynamics can potentially impact the wake characteristics. Wind tunnel tests with a scaled wind turbine model were conducted in [3], simulating surge motion of a FOWT. When the average axial-speed deficit at 2.3D (rotor diameter) was investigated, the authors did not find any clear evidence of improved wake recovery due to additional surge motions.

High-fidelity simulations are also used to calibrate wake models for full-scale turbines. As presented in [4] and [5], an optimization-based calibration and validation of the medium-fidelity wind farm modeling tool, FAST.Farm, against LES was conducted. The advancements in lidar technology has enabled wake measurements of full-scale turbines, as demonstrated in studies [6, 7, 8, 9, 10]. In a recent study [11], the wake condition of a 6MW FOWT from Hywind Scotland was captured using a scanning lidar. The integration of real-world measurements and simulations contributes to a better understanding of the wake phenomena.
In this study, we explore the possibility of measuring the near-wake of a FOWT using a short-range nacelle-based lidar system with the following objectives:

- Assessing the capability of a four-beam nacelle-based lidar system to measure the near wake of a FOWT.
- Understanding the quasi-static near-wake of a full-scale FOWT.
- Evaluating the numerical modeling accuracy of the near-wake using lidar simulations.

We present field measurements acquired by a four-beam nacelle-based lidar. Additionally, we incorporate lidar simulations using FAST.Farm and the panel method-based *pan*MARE as numerical solvers.

2 Methodology

This section is divided into three parts, each addressing critical aspects of our research methodology. Firstly, we provide an overview of the physical setup used to capture the wind field behind the turbine and explain the data processing methods. A parametric study on the field measurements is then conducted to identify key parameters influencing the lidar observations. Following this, we detail the specific simulation cases considered in our study, outlining the criteria for case selection. Lastly, we introduce the numerical frameworks, outlining the simulation models utilized for both the FOWT and lidar simulations.

2.1 Experimental measurement setup and environmental parameter categorization

The wake measurement campaign was conducted on the Floatgen[1], a 2MW FOWT demonstrator located at SEMREV[2], which had no surrounding obstacles. It took place from February to the end of May in 2023. The commercial nacelle-based lidar, WindIris[3], and the setup for inflow measurements were detailed in a previous study [12]. In the present study, this lidar was rotated 180 degrees to measure the wake, and the optical head was re-aligned to account for the quasi-static pitch angle of the floater during operation. The top, side and front views of the measurement setup including the lidar beams are illustrated in figure 1 (a-c), whereas combinations of beams used in data plotting and analysis are shown in (d-g). Each beam is represented by its number (0-3) and the measurements are presented in terms of 10-minute mean radial wind speeds (RWS). The blue circles represent the measurement points located at the center of the lidar range gates. The lidar captured measurements up to 2.5D distance.
It is important to note that we do not present the field measurements in the conventional representation of the wake, which is usually represented in the same plane. In the present study, lidar measurements were not taken in the same horizontal or vertical plane. Instead, measurement points along the beams are located at different heights and downwind distances.
Wave information was obtained from the European Marine Observation and Data Network[4]. The 30-minute spectral significant wave height (H_s), peak wave period (T_p) and wave direction were linearly interpolated for each 10-minute, and used in the present study.
A visual inspection of the lidar measurements was carried out to investigate the sensitivity of the lidar observations to environmental conditions. Turbulence intensity, vertical shear exponent (α) and significant wave height were chosen as parameters of interest. The turbulence intensity has strong

[1] https://www.bw-ideol.com/en/floatgen-demonstrator. Accessed on 23.01.2024.

[2] https://sem-rev.ec-nantes.fr/. Accessed on 23.01.2024.

[3] https://www.vaisala.com/sites/default/files/documents/WindIrisTurbineControlBrochure.pdf. Accessed on 23.01.2024.

[4] https://map.emodnet-physics.eu/platformpage/?platformid=63ea35153372ba001f5f6abf&source=cp. Accessed on 07.08.2023.

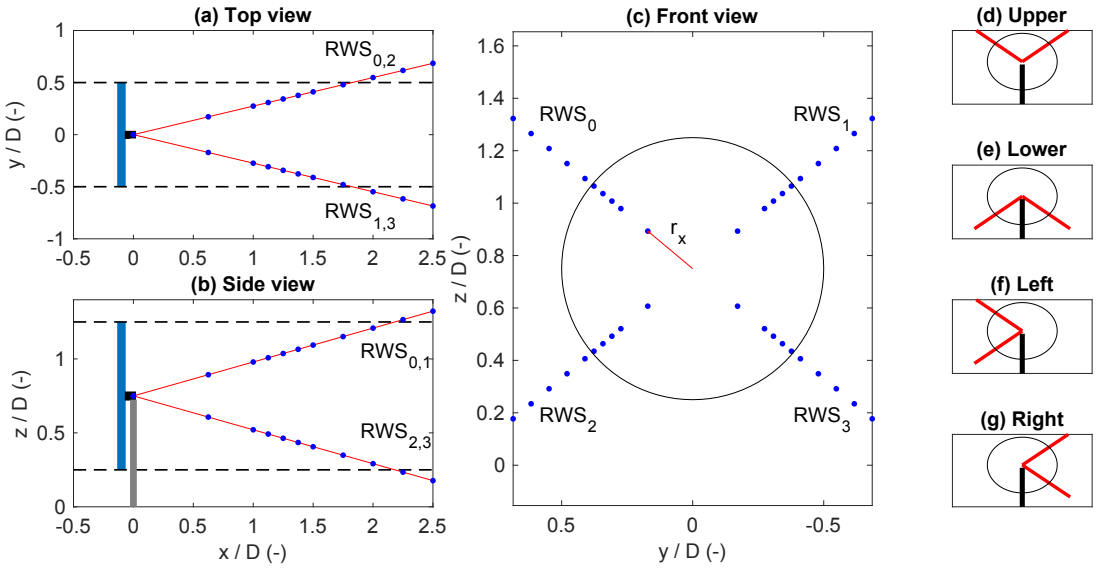

Figure 1: Sketch of the nacelle-lidar orientation and measurement distances. Blue circles represent measurement points in space. Sub-figures (a), (b) and (c) represents top, side and front view, whereas (d-g) describe the beam combinations for which the measurements are presented.

impact on the wake mixing with the undisturbed flow. The vertical wind shear is important due to the configuration of the measurement system, because each measurement point along a given beam is at a different height. The significant wave height influences the motions of the lidar mounted on top of the FOWT. The average environmental characteristics and their chosen ranges are given in table 1.

Table 1: Measurements categorized into 10-minute average flow characteristics at 2.5D, and wave characteristics and their respective chosen ranges given in parentheses.

Name	*Sample count*	U_{hub} (m/s)	α $(-)$	TI (%)	T_p (s)	H_s (m)
LT	20	7.1 (6.5-7.5)	0.03 (0.00-0.06)	4.4 (1.5-5.5)	10 (9-12)	1.3 (0.9-2)
HT	16	6.9 (6.5-7.5)	0.03 (0.00-0.06)	7.2 (6.5-10.5)	10 (9-12)	1.3 (0.9-2)
LS	15	7.1 (6.5-7.5)	0.03 (0.00-0.06)	4.1 (1-5)	10 (9-12)	1.3 (0.9-2)
HS	3	7.0 (6.5-7.5)	0.17 (0.12-0.24)	4.2 (1-5)	11 (9-12)	1.3 (0.9-2)
LHs	6	6.8 (6.5-7.5)	0.02 (0.00-0.06)	6.6 (5-9)	10 (9-12)	0.9 (0.0-1.0)
HHs	7	7.1 (6.5-7.5)	0.04 (0.00-0.06)	6.3 (5-9)	11 (9-12)	1.8 (>1.6)

The lidar reconstructed hub-height wind speed (U_{hub}) and RWS from the lidar were utilized in the present study. Measurements around an average hub-height wind speed of 7 m/s were chosen to focus on the below rated region. Focusing on below-rated conditions in wake studies is essential, because it is the operating range that has the largest impact on the energy production in a wind farm. We filtered out time periods where the difference between RWS measurements at 2.5D and 0.75D was less than 2 m/s and considered them as flow without wake. TI is calculated from the reconstructed wind speed at 2.5D. Floater motion-induced velocities in RWS measurements in the range of wave frequencies are filtered out in the frequency domain before the calculation of TI. Lidar reconstructed vertical shear exponents were calculated based on power law between the upper and lower beams at 2.5D. The wind direction for the rotor-aligned cases were selected based on the lidar reconstructed hub-height wind direction at 2.25D and 2.5D in a range of 0 ± 2 degrees. This was necessary to differentiate symmetric and highly non-symmetric wakes and filter out misaligned operation cases. It is important to note that the lidar reconstruction of the wind field relies on the assumption of a homogeneous wind field, a condition not met within the wake. This, coupled with the limited information available on the environment and the turbine, introduces uncertainties in the lidar reconstructed wind field.

Significant wave height, peak wave period and wave direction were also taken into account in the categorization. The range of wave characteristics were chosen based on the results of numerical model validation studies in the VAMOS project to reduce uncertainties in turbine response as much as possible. The range of wave directions was limited around the dominant direction of the site, which was around 260 degrees.
In figure 2, the velocity profiles of three categories with changing TI, α, and H_s were normalized to their respective U_{hub}. The average of all 10-minute mean RWS is plotted against the corresponding radial distance, r_x. The upper two-beam measurements for varying TI and H_s, and the left side beam measurements for varying α were investigated. The lidar observations did not exhibit clear differences between variations in TI. Moreover, there was no clear indication that the motion of the floater was causing any additional mixing of the wake. A possible uncertainty in this comparison is the lack of wind-wave misalignment information, and the resulting pitch and roll motions. Due to the inhomogeneity of the wake field, the averaging of RWS due to motions could have distinct effects at different measurement points. For instance, a measurement point at the peaks of a double Gaussian shape would observe a higher wind speed when pitch motion is introduced. The measurements were highly susceptible to changes in vertical shear due to each point being located at a different height.

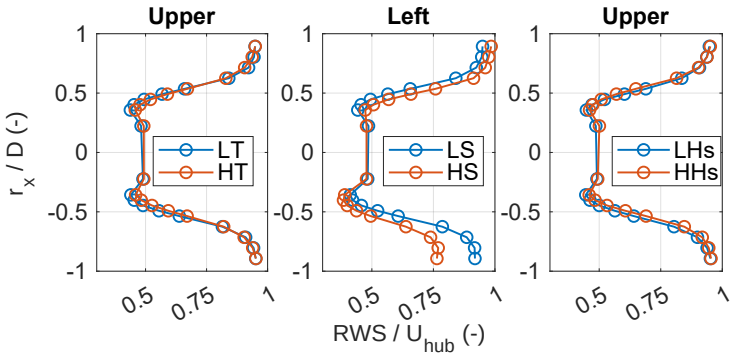

Figure 2: Comparison of 10-minute average RWS of changing TI, α, and H_s normalized to their respective U_{hub}; given from left to right respectively.

2.2 Simulation case selection

Based on the results of the environmental parameter categorization, different combinations of TI and α were grouped to encompass three distinct atmospheric conditions while considering the data availability within the specified ranges. Table 2 shows the range of the average environmental conditions, categorized into five groups to capture low turbulence (LT)-high shear (HS), medium turbulence (MT)-medium shear (MS), high turbulence (HT)-low shear (LS), as well as low and medium yaw misalignment (LY, MY). The "sample count" refers to the number of 10-minute measurement periods in each category. The case matrix contains reasonable variability of TI and α and also includes the yaw-misaligned ($\theta_{mis.}$) cases to cover representative offshore conditions. For the yaw-misaligned cases, the lidar reconstructed hub-height wind directions at 2.5D were filtered for -4 ± 1 degrees and -8 ± 1 degrees.

2.3 Numerical simulation models

2.3.1 FAST.Farm and ViConDAR The FOWT, Floatgen, was modeled in OpenFAST and verified in [13, 14]. The hydrodynamic coefficients of the simulation model were further calibrated based on full-scale measurements. This model was used in the present study and simulations were carried out using FAST.Farm v3.3.0[5] with wind fields created by TurbSim v2[5]. FAST.Farm uses an improved dynamic wake meandering model, that makes use of several parameters to describe the near wake velocity deficit [4]. Several parameters affect the wake deficit and correct for the pressure gradient zone in the near-wake. In the present study, we used default settings for the wake model parameters.
Wake wind fields with 3 meters grid spacing were extracted from the FAST.Farm simulations at nine downwind distances while taking the quasi-static surge position into consideration. The extracted

[5]https://github.com/OpenFAST/openfast. Accessed on 23.01.2024.

Table 2: Definition of simulation cases where inputs were selected as 10-minute average flow characteristics at 2.5D, and wave characteristics based on field measurements, with their respective chosen ranges given in parentheses.

Name	*Sample count*	U_{hub} (m/s)	α $(-)$	TI (%)	T_p (s)	H_s (m)	$\theta_{mis.}$ (deg)
LT-HS	8	7.2 (6-8)	0.15 (0.12-0.24)	4.0 (1-5)	10 (7-12)	1.9 (1.5-3)	0 (-2-+2)
MT-MS	11	6.9 (6-8)	0.07 (0.06-0.12)	6.3 (5-9)	11 (9-12)	1.6 (1-2)	0 (-2-+2)
HT-LS	9	6.6 (6-8)	0.03 (0.00-0.06)	9.4 (8-12)	12 (9-14)	0.9 (0.5-1.5)	0 (-2-+2)
LY	7	6.7 (6-8)	0.08 (0.06-0.12)	5.4 (3-7)	11 (9-14)	1.6 (1-2)	-4 (-5 - -3)
MY	6	7.2 (6-8)	0.11 (0.06-0.12)	4.3 (3-7)	12 (9-14)	1.5 (0.9-2.1)	-8 (-9 - -7)

planes were at the same downwind distance as real measurements, except for the missing plane at 1.125D. This was due to the limitation of the used FAST.Farm version, which only allowed the extraction of 9-downwind planes. Lidar measurements in the wake wind fields were simulated using ViConDAR, which was adapted to include the six-degrees of freedom of the nacelle dynamics [15]. Unlike inflow lidar simulations, Taylor's frozen turbulence hypothesis does not apply in wake due to wake recovery effects. Therefore, within the probe volume of the lidar simulations, wake recovery is not captured. The lidar simulator calculates the line of sight velocity as the average of the focus points in the probe volume. FAST.Farm simulations were carried out with turbulent wind and irregular waves. The dominant wave direction, which is around -22.5 degrees misalignment to the wind, was chosen for the simulations. Each case is simulated for a single random seed of wind and waves for 1200 seconds with wind and wave fields repeating at 600 seconds. The last 600 seconds were used to calculate statistics. It would be worthwhile to investigate the simulation of each sample. However, the computational time required for *pan*MARE was too time consuming for this study.

2.3.2 panMARE with lidar simulator The first-order panel method *pan*MARE is an in-house development of the Hamburg University of Technology, which was extended to the simulation of FOWT by Netzband et al. [16]. During the VAMOS project, a validation and verification of *pan*MARE with full-scale measurement data and simulations of the Floatgen prototype has been performed [13]. A so called 'hybrid validation' was carried out, which allowed to compare the aerodynamic loads directly while the modeled turbine followed the exact motion trajectory of the real FOWT. In the considered case, maximum deviations of 10% between simulations and time series measurement data were observed in rotor torque and rotor speed. In addition, the influence of the wave-induced motions on the aerodynamic loads was captured accurately. The panel method is a boundary element method where the blade surface is discretised by source and doublet panels, while the freely transported three-dimensional wake is represented by doublet panels only. It is based on the potential flow theory, that describes the flow field as a boundary value problem. The drawback of this formulation is that the viscosity is not considered. Therefore, viscous drag forces are added by a viscous correction, which is based on empirical, two-dimensional drag coefficients of the blade sections.
A more detailed description of the panel method itself in conjunction with wind turbine rotors can be found in [16], while the utilized rotor model and the viscous correction is described in another investigation focusing on the unsteady aerodynamic effects of FOWT [14]. To avoid singularities in the wake field caused by the doublet panels, a viscous vortex core based on the Lamb-Oseen model is used in the wake. The vortex core radius in the present simulations corresponds to 5% of the rotor diameter. No vortex core growth model is applied.
The four lidar beams are modeled as geometric objects rigidly connected to the nacelle. Therefore, the motion of the lidar beams due to the platform motion is exactly captured. The flow and motion velocity along the beams is exported and post-processed in the lidar simulator, which is part of *pan*MARE. The lidar simulator computes the line of sight velocities along the beam including the motion velocity of the nacelle at each position on the moving beam. For the sake of comparability with the ViConDAR simulations, the gate velocity is computed by averaging the velocity over the probe length without any weighting.
To ensure that the numerical models are comparable, the motion of the FOWT was not directly calculated in *pan*MARE, but was forced to follow the motion obtained by FAST.Farm. This is similar to the concept of a 'hybrid validation', which was successfully tested in the above mentioned validation work within the VAMOS project [13].

3 Results and discussion

In this section we present the comparison of measurements and simulations for the five cases, analyse and discuss the observed differences. This section is divided into two clusters of cases as shown in table 2: Aligned and misaligned operation and quantification of errors. In the following figures, RWS are plotted against the corresponding radial distance, r_x. They are represented as a combination of two beams out of four as previously described in figure 1. The average of all 10-minute mean RWS are represented as black circles and denoted as *Field*. The shaded areas represent the minimum and maximum of 10-minute mean RWS for the given measurement point. FAST.Farm and ViConDAR simulations are denoted as *FAST+VCD* and *pan*MARE with its lidar simulator as *panMARE*. Red and blue crosses are the 10-minute average RWS from *FAST+VCD* and *panMARE* simulations, respectively.

3.1 LT-HS, MT-MS and HT-LS cases

The simulations and field measurements are plotted against each other for the LT-HS case in figure 3. The *Field* lidar observes a symmetric wake at the upper beams, but the same is not the case for the lower beams. This difference can also be seen when the left and right side beams are compared. *FAST+VCD* simulations predict more of a single Gaussian shape compared to the double Gaussian observed in the field measurements. In the FAST.Farm waked wind fields, it is possible to observe the double Gaussian deficit shape. Thus, possible reasons that it is not apparent in the lidar simulations could be that the motion-induced averaging in the lidar measurements is overestimated in the simulations, thus reducing the deficit at the Gaussian peaks. Another reason could be that *FAST+VCD* simulations predict a smaller pressure gradient zone behind the rotor. *FAST+VCD* shows the best agreement with the upper beams, despite a slight shift of the wake towards the left (positive r_x/D) side. This difference could have been caused by the presence of veer, a statistical error due to the small number of samples or an inaccurate calibration of the wake deflection model. Veer, which is the wind direction change over height, is a possible disturbance that could have affected the lidar measurements by introducing a slight deflection throughout the rotor. Simulation predictions showed less agreement at the two lower beams, in particular at the lower left beam. Here, the simulations largely underestimate the wake deficit. One possible explanation could be that the upwards deflection of the wake center, caused by the floater pitch and rotor tilt, is overestimated by *FAST+VCD*.

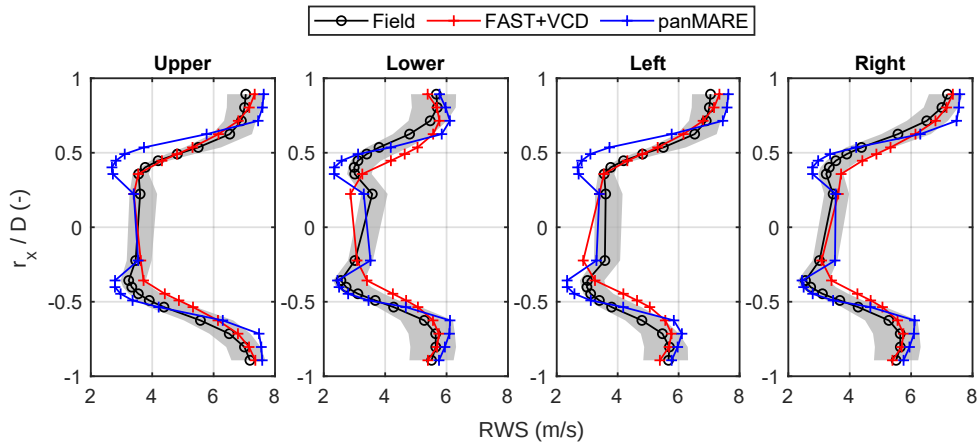

Figure 3: RWS from the LT-HS case plotted against their corresponding radial distance from the rotor center, where the shaded area represents the minimum and maximum of the 10-minute averages.

In the *panMARE* results the double Gaussian shape is clearly observed. However, it overestimates the velocity deficit around the Gaussian peaks. This is most likely caused by two reasons: First, there is no model implemented in the panel method simulations to account for the displacement and the turbulent region behind the nacelle. This allows the flow to accelerate in the nacelle region, which in turn yields a slightly higher velocity deficit behind the blades. Second, the vortices in the panel method are generally conserved over time. Therefore, typical viscous phenomena occurring in a wind turbine wake such as the mixing of the wake with the atmospheric flow or vortex core growth are not captured in the model. This leads to a stronger velocity gradient from the inner part of the wake to the free stream, which yields an overestimation of the wake deficit at the outer blade sections. Since the measurement points

at $r_x/D = 0.5$ are located around 1.7 D behind the rotor, the influence of this and other viscous effects are most likely significant in this area. For the same reason, the free-stream velocity is generally reached at lower r_x/D in comparison to the measurements and FAST.Farm simulations.
In addition, a discrepancy of the measured RWS at the last point of the upper lidar beams and the *panMARE* simulations is visible in figure 3. As the discrepancy between measurements and *panMARE* cannot be observed consistently in the following simulations, the presence of a systematic influence on the comparisons is unlikely. This difference might be caused by inaccuracies of the wind field reconstruction using the lidar. Similarly, a difference between *FAST+VCD* and *panMARE* is visible. A possible explanation is that in *FAST+VCD* results, the wind speed is not yet fully converged to the undisturbed wind speed, whereas it is for *panMARE*.
Unlike the LT-HS case, *Field* observations of the HT-LS case do not exhibit the asymmetry as shown in figure 4. Compared to the previous case, *FAST+VCD* predict closer to the observations for the upper beams, while still producing a single Gaussian shape. Similar to the previous case, *panMARE* overestimates the velocity deficit around the Gaussian peaks and the wake recovery towards the end of the wake diameter.

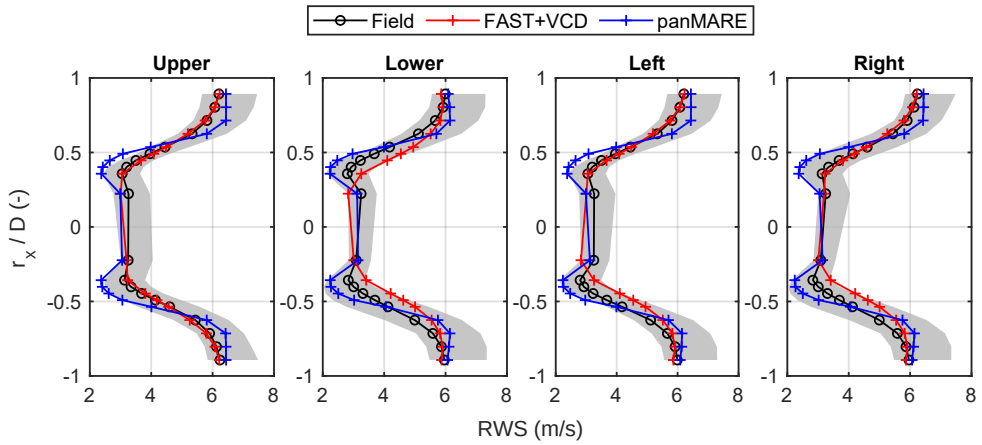

Figure 4: RWS from the HT-LS case plotted against their corresponding radial distance from the rotor center, where the shaded area represents the minimum and maximum of the 10-minute averages.

Detailed results for the MT-MS case are not shown here, since they are very similar to those of HT-LS. More information on the prediction accuracy of all cases is presented at the end of this section.

3.2 LY and MY cases

Figure 5 shows the comparison of field measurements and simulations for the case LY ($\theta_{mis.} = -4$ degrees) case. Here, the field measurements show a higher variation between the 10-minute averages, visible as a larger shaded area. This could be due to the methodology of wind direction reconstruction, which relies on the homogeneous wind field assumption. This assumption is not valid in the near-wake, especially in the case of a yaw misalignment.
Nevertheless, it is possible to observe the wake during misaligned operation in both the field and simulated measurements. Here, the wake moves out of the side of the left beams towards the right due to the yaw misalignment of the lidar with the mean wind speed and wake deflection. Therefore, the double Gaussian shape of the near-wake is more apparent on the right beams for the *Field* measurements, *FAST+VCD* and *panMARE* simulations. In accordance with the previous results, the *FAST+VCD* simulations are more accurate for the upper beams and less accurate for the lower left beam, where it mostly underestimates the velocity deficit. The *panMARE* estimations show similar trends to the previous cases, except for the estimations at closest measurement point at lower right beam. As the *pan*MARE simulations does not include a hub model, the flow in the blade root region can pass through the nacelle region unobstructed. Due to the yawed inflow, the inner measurement point of the lower right beam enters this region, which leads to a non-physical velocity.
Measurements of the MY ($\theta_{mis.} = -8$ degrees) case show a lower variation compared to LY as shown in figure 6. Here, the convergence to the undisturbed wind speed is even more apparent for the left beams. The simulation results are similar to those of the LY case, except for the non-physical velocity predicted

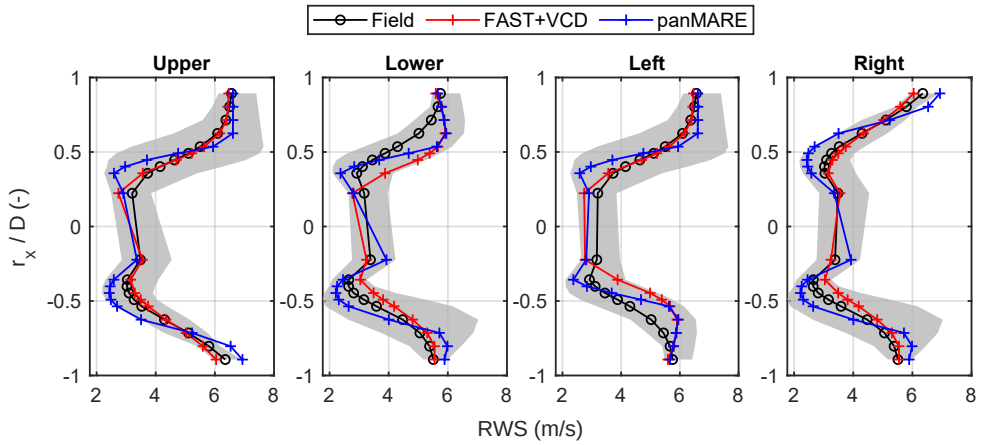

Figure 5: RWS from the LY case plotted against their corresponding radial distance from the rotor center, where the shaded area represents the minimum and maximum of the 10-minute averages.

by *panMARE* at the closest measurement point on the lower right beam exhibits is greater than in the LY case.

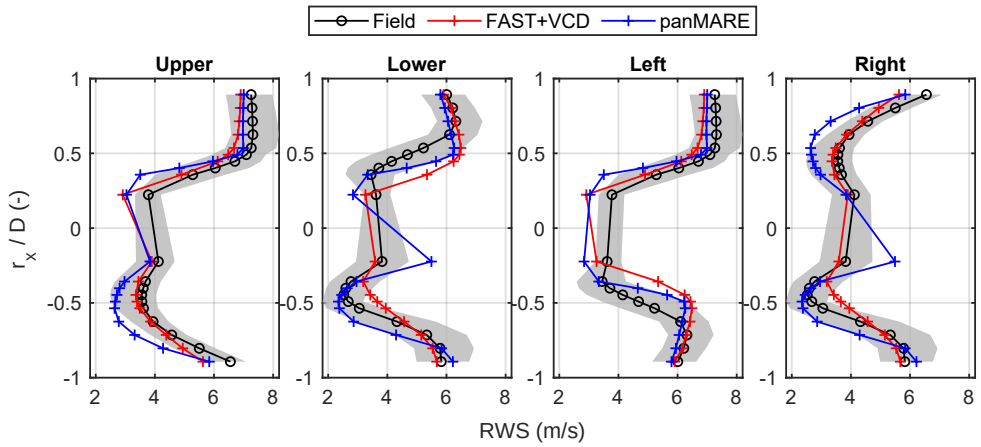

Figure 6: RWS from the MY case plotted against their corresponding radial distance from the rotor center, where the shaded area represents the minimum and maximum of the 10-minute averages.

3.3 Error quantification

The Mean Absolute Percentage Error (MAPE) is calculated between the average of the field measurements samples and simulations of each case for the four beam combinations to quantify the differences between measurements and simulations. For a given beam combination per case, the MAPE is calculated as:

$$MAPE = \frac{100\%}{N} \sum_{i=0}^{N-1} \frac{|\overline{RWS_i} - \hat{RWS_i}|}{\overline{RWS_{2.5D}}}, \tag{1}$$

where $\overline{RWS_i}$ is the average of all $field$ mean RWS, $\hat{RWS}$ is the simulated mean RWS at a given measurement point, and N is the number of common available measurement points between the measurements and simulations. The results for the five cases are shown in figure 7.
In general, *FAST+VCD* was able to represent the upper beams with errors ranging from 1.4% to 5.7%. On the other hand, the lower beam predictions were worse with errors ranging from 7.8% to 11.2%.

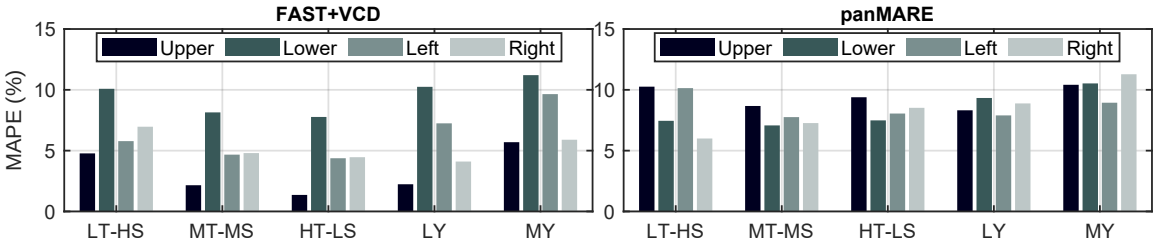

Figure 7: Mean absolute percentage error between the average *Field* radial wind speed measurements, and *FAST+VCD* and *panMARE* simulations.

panMARE had a similar error range for all beam combinations ranging from 6.0% to 11.3%. *FAST+VCD* estimates were mostly within the scatter of the field measurement samples and overall showed a better prediction of the measurements than *panMARE*. *FAST+VCD* estimates were closer to measurements at lower vertical shear exponents and wind aligned operation. Similar to *FAST+VCD*, *panMARE* also showed higher error at high yaw misalignment. However, in wind aligned operation, similar errors were observed in all three cases.

4 Conclusions

This study relied solely on lidar measurements for the reconstruction of wind fields. Therefore, limitations such as wind speed, turbulence intensity, wind direction estimations in a non-homogeneous wind field using lidar or the lack of atmospheric stability information introduce uncertainties to the analysis. Moreover, the simulations did not include the true wind direction and the nacelle yaw angle, and the measurements are filtered to match certain expected conditions.

Nevertheless, we have shown that this measurement setup can be used to measure the near-wake of a floating offshore wind turbine. The double Gaussian shape of the near-wake in aligned and yaw misaligned conditions was observed in the measurements. Lidar measurements were more sensitive to vertical shear than turbulence intensity or significant wave height, possibly because the lidar focus points were at different heights. The influence of floater motions could only be investigated via the significant wave height due to the lack of floater motion data. This limitation may lead to over- or underestimation at different locations in the wake due to the averaging effects. However, using only the significant wave height as a filter, no clear differences were observed in the lidar measurements in the wake.

Three combinations of turbulence intensity, vertical shear in wind-aligned operation and two yaw-misaligned operations were categorized from the measurements and their average characteristics were simulated. Engineering wake models incorporated in FAST.Farm combined with the lidar simulator ViConDAR and the panel method based *pan*MARE with its lidar simulator were used to reproduce the measurements. *FAST+VCD* was able to reproduce the RWS measurements within a mean absolute error range of 1.4%-11.2% and *panMARE* within a range of 6.0%-11.3%. *FAST+VCD* performed worse at lower beam measurements while *panMARE* performed similarly overall. Although both models were able to simulate measurements during yaw misalignment, they exhibited the largest errors in these cases.

This study demonstrates the feasibility of using a four-beam nacelle-based lidar for near-wake measurements on a FOWT for a selected set of environmental conditions. The ability to measure and simulate the near-wake with short-range lidars opens up practical avenues for advancing wind energy research and its applications. The successful field measurements and simulations within the near-wake zone suggest a plausible extension to the far-wake using forward looking lidars in wind farms, allowing for the exploration of lidar-assisted control in waked flow conditions.

Acknowledgments

The research leading to these results is part of the VAMOS project (grant no. 03EE2004A and 03EE2004C), funded by the German Federal Ministry for Economic Affairs and Climate Action (BMWK). The installation of the nacelle-based lidar is also supported by the European Union's Horizon 2020 research and innovation programme under grant agreement number 731084 (MaRINET2) at the SEM-REV test infrastructure. The authors would like to thank BW Ideol for granting access to Floatgen and for technical support throughout the measurement campaign. The authors would also like

to thank Raphaël Adam for his assistance in building the numerical model of the turbine; Sebastian Putzke for technical assistance, and Quentin Guiho for on-site and technical assistance in positioning the nacelle-based lidar.

References

[1] Jonkman J M, Annoni J, Hayman G, Jonkman B and Purkayastha A 2017 Development of FAST.Farm: A New Multi-Physics Engineering Tool for Wind-Farm Design and Analysis *35th Wind Energy Symposium* January (Reston, Virginia: American Institute of Aeronautics and Astronautics) ISBN 978-1-62410-456-5 URL https://arc.aiaa.org/doi/10.2514/6.2017-0454

[2] Campagnolo F, Molder A, Schreiber J and Bottasso C L 2019 *Journal of Physics: Conference Series* **1256** 012006 ISSN 1742-6588 URL https://iopscience.iop.org/article/10.1088/1742-6596/1256/1/012006

[3] Fontanella A, Zasso A and Belloli M 2022 *Journal of Physics: Conference Series* **2265** 042023 ISSN 1742-6588 URL https://iopscience.iop.org/article/10.1088/1742-6596/2265/4/042023

[4] Doubrawa P, Annoni J R and Jonkman J M 2018 *Optimization-Based Calibration of FAST.Farm Parameters against Large-Eddy Simulations* (Reston, Virginia: American Institute of Aeronautics and Astronautics) ISBN 978-1-62410-522-7 URL https://arc.aiaa.org/doi/10.2514/6.2018-0512

[5] Jonkman J, Doubrawa P, Hamilton N, Annoni J and Fleming P 2018 *Journal of Physics: Conference Series* **1037** 062005 ISSN 1742-6588 URL https://iopscience.iop.org/article/10.1088/1742-6596/1037/6/062005

[6] Trabucchi D, Trujillo J J and Kühn M 2017 *Energy Procedia* **137** 77–88 ISSN 18766102

[7] Doubrawa P, Debnath M, Moriarty P J, Branlard E, Herges T G, Maniaci D C and Naughton B 2019 *Journal of Physics: Conference Series* **1256** ISSN 17426596

[8] Zhan L, Letizia S and Iungo G V 2020 *Wind Energy Science* **5** 1601–1622 ISSN 23667451

[9] Reinwardt I, Schilling L, Dalhoff P, Steudel D and Breuer M 2020 *Wind Energy Science* **5** 775–792 ISSN 23667451

[10] Conti D, Dimitrov N, Peña A and Herges T 2020 *Journal of Physics: Conference Series* **1618** ISSN 17426596

[11] Angelou N, Mann J and Dubreuil-Boisclair C 2023 *Wind Energy Science Discussions* **2023** 1–35 URL https://wes.copernicus.org/preprints/wes-2023-37/

[12] Özinan U, Liu D, Adam R, Choisnet T and Cheng P W 2022 *Journal of Physics: Conference Series* **2265** ISSN 17426596

[13] Netzband S, Schulz C W, Özinan U, Adam R, Choisnet T, Cheng P W and Abdel-Maksoud M 2023 *Journal of Physics: Conference Series* **2626** 012061 ISSN 1742-6588 URL https://iopscience.iop.org/article/10.1088/1742-6596/2626/1/012061

[14] Schulz C W, Özinan U, Netzband S, Cheng P W and Abdel-Maksoud M 2023 *Journal of Physics: Conference Series* **2626** 012064 ISSN 1742-6588 URL https://iopscience.iop.org/article/10.1088/1742-6596/2626/1/012064

[15] Gräfe M, Pettas V and Cheng P W 2022 *Journal of Physics: Conference Series* **2265** 0–12 ISSN 17426596

[16] Netzband S, Schulz C W, Göttsche U, González D F and Abdel-Maksoud M 2018 *Ship Technology Research* **65** 123–136 ISSN 0937-7255